Formation mechanism and Growth of $MNbO_3$, M=K, Na by *in situ* X-ray diffraction

Susanne Linn Skjærvø[a], Sanna Sommer[b], Peter Nørby[b], Espen Drath Bøjesen[b], Tor Grande[a], Bo B. Iversen[b] and Mari-Ann Einarsrud[a]*

[a]Department of Materials Science and Engineering, NTNU Norwegian University of Science and Technology, Trondheim, Norway

[b]Center for Materials Crystallography, Department of Chemistry and iNANO, Aarhus University, Denmark

*Corresponding author:

Mari-Ann Einarsrud

mari-ann.einarsrud@ntnu.no

phone: +47 48136521

fax: +47 73550203

Abstract

Hydrothermal synthesis is a well-established method to produce complex oxides, and is a potential interesting approach to synthesize stoichiometric lead-free piezoelectric $K_{0.5}Na_{0.5}NbO_3$. Due to challenges in obtaining the desired stoichiometry of this material, more knowledge is needed on how the end members, $KNbO_3$ and $NaNbO_3$, are nucleating and growing. Here we report on the formation mechanisms and growth during hydrothermal synthesis of $KNbO_3$ and $NaNbO_3$ by *in situ* synchrotron powder X-ray diffraction. We show that tetragonal $KNbO_3$ crystallites form from dissolved T-Nb_2O_5 at 250-300 °C and 250 bar while orthorhombic $NaNbO_3$ forms *via* several crystalline intermediate phases at 225-325 °C and 250 bar. The crystallite size of $KNbO_3$ is decreasing while the crystallite size of $NaNbO_3$ is increasing with increasing temperature, demonstrating that the presence of intermediate phases is highly important for the nucleation and growth of the final product. The different crystallization schemes explains the challenge in obtaining stoichiometric $K_{0.5}Na_{0.5}NbO_3$ by hydrothermal synthesis.

Introduction

Environmental and health concerns have stimulated an increasing interest for developing lead-free piezoelectric materials[1]. $K_{0.5}Na_{0.5}NbO_3$ (KNN)-based materials are a promising lead-free alternative[2]. The end members, $KNbO_3$ and $NaNbO_3$, additionally, have interesting functional properties; $KNbO_3$ is a ferroelectric material[3] and $NaNbO_3$ is antiferroelectric[4]. $NaNbO_3$ forms solid solutions with $KNbO_3$ and thus enhancing the piezoelectric properties, but the stoichiometry is crucial to achieve the desired piezoelectric response[2].

Hydrothermal synthesis generally employs moderate temperature (usually 150-400 °C) combined with high pressure (usually below 250 bar) to form nanocrystalline powders of high crystallinity and controlled crystallite size[5,6]. The stoichiometry control of $K_xNa_{1-x}NbO_3$ has, however, shown to be a challenge as potassium and sodium will enter the structure at different rates[7,8]. Hence, knowledge of the formation of the end members, $KNbO_3$ and $NaNbO_3$, under hydrothermal conditions would be beneficial. Despite extensive use of hydrothermal methods (*e.g.* regular autoclave synthesis with and without stirring, microwave assisted hydrothermal synthesis and pulsed hydrothermal synthesis), general knowledge on the nucleation and growth processes is still limited. Valuable knowledge has been obtained through *ex situ* studies[9-15] where the reactions are stopped mid-way, but these studies cannot fully reveal the real-time process in the vessel. Therefore, efforts have been made during recent years to study the hydrothermal synthesis by *in situ* methods. Such studies are challenging, as they require a reaction vessel penetrable to X-rays while also being strong enough to maintain the desired hydrothermal pressure. To the authors' knowledge, only Modeshia *et al.*[16] have previously performed *in situ* studies on the hydrothermal synthesis of $NaNbO_3$. However, energy-dispersive X-ray diffraction (EDXRD) with white-beam synchrotron X-rays were used to describe the process inside a laboratory-sized autoclave giving diffractograms of low quality. Their results indicated that following the dissolution of

the Nb_2O_5 precursor in a solution of 1 M NaOH, the formation of $Na_7HNb_6O_{19}\cdot 15H_2O$ and $Na_2Nb_2O_6\cdot nH_2O$ ($n \approx 1$) in addition to an unknown intermediate phase could be observed during the hydrothermal synthesis at 240 °C. The intermediate phases are the result of strong alkaline solutions dissolving the solid Nb_2O_5 precursor, rendering a range of new species dependent on the pH of the solution.[17] At pH between 6.5 and 11.5 the protonated hexaniobate ion $H_xNb_6O_{19}^{8-}$ (x=1-3) will form. In the presence of sodium and potassium ions formation of potassium and sodium hexaniobate hydrates occur. Sodium gives the lowest solubility compared to potassium of these species in water.[7]

Here we present the first synchrotron *in situ* powder X-ray diffraction (PXRD) study investigating the formation mechanisms of $KNbO_3$ and $NaNbO_3$ under hydrothermal conditions. We demonstrate how the differences between the two material systems can affect the reaction mechanisms. By using a small capillary as the reaction vessel, highly homogenous and controllable conditions were achieved, enabling general knowledge on hydrothermal processes to be extracted.

Experimental procedure

The Nb_2O_5 precursor was made by precipitation from $(NH_4)NbO(C_2O_4)_2\cdot 5H_2O$ (0.25 mol, Sigma-Aldrich, 99.99 %) by using NH_4OH (25 wt%, Emsure) as described by Mokkelbost *et al*.[18] The mixture was dried at 80 °C in a Rotavapor and then heated to 600 °C for 12 h before being gently ground. The particle size was determined using a Hitachi S-3400N scanning electron microscope (SEM) and confirmed by *in situ* synchrotron PXRD.

Highly concentrated slurries were made to maximize the signal to noise ratio for the *in situ* XRD measurements. *For the K-Nb-O system*: T-Nb_2O_5 powder (0.0039 mol) and KOH (0.038 mol, Merck) were added to distilled H_2O (3.5 mL) giving a [KOH] = 10.6 M and [K]/[Nb] = 9.6. *For the Na-Nb-O system*: NaOH was used (0.052 mol, Merck) giving a

[NaOH] = 14.3 M and [Na]/[Nb] = 13.6. The slurries were mixed well in an agate mortar and then injected into the *in situ* cell by using a plastic syringe.

In situ PXRD data were recorded at beamline I711 at MAX II, Lund, Sweden[19] using a monochromatic beam with wavelength of 0.99 Å. The *in situ* cell, previously described by Becker *et al.* [20] and Jensen *et al.* [21] consisted of a single-crystal sapphire capillary with an outer diameter of 1.15 ± 0.1 mm and inner diameter of 0.8 ± 0.1mm connected to Swagelok® fittings with graphite ferrules which were stabilized by an adjustable steel frame. Pressure was provided by an HPLC pump connected to one end of the capillary, while the other end was closed. A volume of the sapphire capillary was heated by a hot air gun to reach sub- and supercritical conditions and the temperature was calibrated using a thermocouple. Even for the highest temperatures, the heating to the set point temperature was within < 20 s.

The capillary was exposed to X-rays and the diffracted signal was detected by an Oxford Diffraction Titan CCD detector with 5 s intervals. The raw data was masked to remove single-crystal sapphire reflections from the capillary, shadow of the beam stop and bad pixels and integrated to yield 1D data in the Fit2D software.[22]

Topas 5 (Bruker AXS, Germany) was used to refine the unit cell parameters and crystallite size. The instrumental resolution function, wavelength calibration and detector distance corrections were performed using a NIST 660a LaB_6 standard. To de-convolute the contributions from peak-splitting and size-broadening, unit cell parameters and crystallite size were extracted using two different methods: **1)** The unit cell parameters were refined by fitting the peaks with the modified Thomson-Cox-Hastings pseudo-Voigt (TCHZ) peak type[23,24] *i.e.* not taking size-broadening into account, refining the scale factor and Chebychev background parameters for each frame, while keeping the zero error fixed to the value refined for the last recorded frame. The isotropic temperature factors and atomic positions were fixed to the literature values of each phase. **2)** All crystallite sizes were extracted by refining the

Lorentzian isotropic size parameter. To remove any contribution from splitting of peaks, the unit cell parameters were fixed to the values found for the last recorded data frame ($NaNbO_3$), or the frame with the best statistics ($Na_2Nb_2O_6 \cdot H_2O$) for each experiment. The scale factor and Chebychev background parameters were refined for each frame but the zero error was fixed to the values found for the last recorded data frame for each experiment. The isotropic temperature factors and atomic positions were fixed to the literature values of each phase.

All refinements were additionally performed in the Fullprof software[25] to reveal information about the broad background features. From the extracted Chebyshev polynomials the broad features in the diffraction patterns in the 2θ-range of 5-37°, was integrated using a commercial software package (MATLAB 8.5, The MathWorks Inc., Natick, MA, 2015a).

Results and discussion

The K-Nb-O system

The formation of $KNbO_3$ was investigated at 250, 275 and 300 °C and 250 bar. The general evolution of phases was determined as well as the crystallite size and the tetragonality of the final product.

The evolution of the phases

A 2D contour plot of the development of phases for the K-Nb-O system at 275 °C and 250 bar is displayed in Figure 1a and shows the general development of the diffraction pattern for all the recorded temperatures. Before the onset of heating, the T-Nb_2O_5 precursor (space group Pbam, no. 55[26]) was observed as seen in detail in Figure 1b. This is identical to the structure of the dry precursor powder as confirmed by *ex situ* PXRD (Figure S1 and Table S1). The particle size of the precursor powder determined by SEM was 50-100 nm (Figure

S2) which corresponds well to the refined value of 92 nm (Table S1). After heating was initiated almost instantaneous dissolution of the precursor occurs (< 20 s) for all the different temperatures. Complete dissolution of the solid precursor was confirmed by video recordings of the capillary during heating. After a period of time (10 to 50 s, dependent on the set-temperature), the diffraction lines of tetragonal $KNbO_3$ (space group P4mm, no. 99[27]) appears at all the temperatures investigated. A Rietveld refinement of the final $KNbO_3$ product phase at 275 °C is shown in Figure 1c. 2D contour plots for the formation of $KNbO_3$ at 250 and 300 °C at 250 bar are compared to the data at 275 °C in the supplementary information (Figure S3). Sequential refinements of the scale factor of $KNbO_3$ (Figure 1d) show that as the set-temperature increases the formation rate of $KNbO_3$ is faster as shown by the initial slope of the curves. At 250 °C a stable scale factor is obtained after approximately 38 min while at 300 °C, stabilization is obtained after approximately 5 min. A stable scale factor shows that the total amount of $KNbO_3$ is constant. For the three temperatures the scale factor stabilizes at different values. As the particles form agglomerates the intensity will depend on the number of agglomerates in the beam, thus the absolute scale factor should be considered arbitrary.

Crystallite size and tetragonality of $KNbO_3$

By refining unit cell parameters and crystallite size simultaneously, a strong correlation between these two parameters was seen. Therefore, two different approaches were used to de-convolute the two contributions. Assuming constant unit cell parameters, the refined crystallite sizes of $KNbO_3$ (Figure 2a) increases with time until a constant size was reached after <5 min, dependent on the temperature. The decreasing crystallite size as the synthesis temperature increases suggests a higher initial nucleation rate at high temperature, resulting in less precursor for each nuclei and hence a smaller crystallite size. A similar trend was observed for $BaTiO_3$-based nanocrystals under hydrothermal conditions by Philippot *et al.*[28]

The time required to obtain an equilibrium crystallite size (Figure 2a) is much smaller than the time for the scale factor to stabilize (Figure 1d) (e.g. 2 min vs 38 min, respectively, at 250 °C). This difference indicates that an equilibrium size is obtained followed by nucleation and growth of new $KNbO_3$ crystallites. When refining the unit cell parameters and neglecting the contribution from the change in crystallite size, a decreasing tetragonality (*c/a*) at higher temperature is observed (Figure 2b) as expected.[29] The lower tetragonality in the early stages of the formation of the crystallites suggests that a finite size effect is suppressing the tetragonal splitting when the particles are small, as also observed by Wang *et al*.[30] for hydrothermally produced $KNbO_3$ nanorods. Similar tetragonality values as shown here were also reported for the nanorods prepared by Wang *et al*. However, these tetragonality values are significantly smaller than the bulk values reported by Shirane *et al*.[29] As the two refinement methods used to find the crystallite size and tetragonality represents two extremes in the description of the physical parameters, information is lacking on the convoluted effect as the broadening of the diffraction lines is probably a result of both change in crystallite size and tetragonality. Hence, higher resolution data acquisition is required to gain further information about this system.

The broad diffraction features

Two broad features are observed in the diffraction patterns in the 2θ-range 5-13° and 13-37° and the integrated area of these is presented in Figure 3. The intensity of the feature in the range 5-13° is constant over time but decreasing with increasing temperature. The intensity of the feature at 13-37° is varying with time and is increasing with increasing temperature, making it clear that the two features arise from two different contributions. The feature in the range 13-37° decreases in two steps. The first decrease seems to be coinciding with the onset of heating, where the T-Nb_2O_5 precursor is dissolving. The time of the second decrease corresponds well with the time for the stabilization of the scale factor as presented in Figure

1d. Therefore, this broad feature is interpreted to be dissolved precursor clusters in the solution, and the concentration of these will decrease as $KNbO_3$ grows. Hence, further increase in the amount of $KNbO_3$ is not possible as the concentration of dissolved precursor clusters is too low.

It should be noted that the area of the broad features is sensitive to the position of the capillary in the beam, affecting the amount of solution and sedimented particles the beam travels through. Also, the capillary moved slightly during the K-Nb-O experiment at 250 °C, but that the movement was deemed to be of minor importance as only the background area seemed to be affected, and to a very small extent.

The Na-Nb-O system

The formation of $NaNbO_3$ was investigated at 225, 250, 275, 300 and 325 °C at 250 bar. The general evolution of phases was determined as well as the structure and crystallite size of the final product.

The evolution of the phases

The 2D contour plot in Figure 4a shows the development of the phases during five different stages in the Na-Nb-O system at 225 °C and 250 bar. Before heating was initiated, stage 1, the T-Nb_2O_5 precursor is observed in addition to the hexaniobate compound $Na_7HNb_6O_{19}\cdot 15H_2O$ described by Anderson *et al.* [31] (Figure S4). At least two unidentified short-lived phases appear during the next 10-30 s (stage 2 and 3) and after 125 s (stage 4) a phase appears that fits well with the $Na_2Nb_2O_6\cdot H_2O$ structure described by Xu *et al.*[31,32] (Figure S5). In less than 4 min the $Na_2Nb_2O_6\cdot H_2O$ crystallites grow to a size of 45 nm (Figure 4b) before the size decreased, suggesting a slow dissolution of $Na_2Nb_2O_6\cdot H_2O$. The $NaNbO_3$ is first observed after 75 s. After 5 min it is the only phase present (stage 5). The same

development in phases is observed at 250, 275, 300 and 325 °C, but at a faster rate (Figure S6). Our results confirm the preliminary data by Modeshia *et al.*[16] using EDXRD showing the presence of $Na_7HNb_6O_{19}\cdot 15H_2O$ and $Na_2Nb_2O_6\cdot H_2O$. In addition, we clearly observe at least two unknown short-lived phases in-between the two phases identified showing an even more complex chemistry of this system than previously reported.

Crystal structure and crystallite size

Refinements on the diffraction patterns of $NaNbO_3$ unequivocally determined the space group to be either Pmmn (no. 59) and Pnma (no. 62), supported by findings of Peel *et al.*[33] The refinement for the Pmmn space group is included in Figure 4c (and in Figure S7). The time to complete conversion to $NaNbO_3$ decreased rapidly with increasing temperature (Figure 5a). Above 300 °C the conversion time approached zero, emphasizing the efficiency of hydrothermal synthesis even at relatively low temperatures. Increasing temperature also results in a higher growth rate of the crystallites and increasing crystallite size of the final product ranging from 77 nm at 225 °C to 198 nm at 325 °C (Figure 5b). This opposite temperature trend compared to $KNbO_3$ could be explained by the presence of the crystalline intermediate phases in the $NaNbO_3$ system, affecting the amount of nuclei formed which can transform into $NaNbO_3$.

The results from this study clearly show the different chemistry of the two end members for KNN formation with respect to phase formation during hydrothermal synthesis. In the sodium system with a lower solubility of the (hexa)niobate species in water several phases nucleate and grow before the final $NaNbO_3$ is formed. Contrary in the potassium system the solubility of the (hexa)niobate phases is so high that no phases precipitate until the $KNbO_3$ is formed. Hence during a hydrothermal synthesis of KNN, the sodium (hexa)niobate will precipitate first and give an inhomogeneous product. To facilitate the formation of phase-pure

KNN, the use of other solvents or mixtures of solvents should be considered to lower the solubility of the potassium (hexa)niobates.

Conclusions

In summary, we have demonstrated for the first time that tetragonal $KNbO_3$ is formed rapidly without the presence of crystalline intermediate phases during hydrothermal synthesis under highly alkaline conditions at 250-300 °C and 250 bar. The final crystallite size of the $KNbO_3$ decreases with increasing temperature. Lower temperature favors a stronger tetragonality of the crystal structure. The low tetragonality in the beginning of the formation of the crystallites might suggest a disorder or finite size effect.

Orthorhombic $NaNbO_3$ forms *via* several crystalline intermediate phases under highly alkaline conditions at 225-325 °C and 250 bar. The time of the reaction and hence the time to obtain single-phase $NaNbO_3$ decreases with increasing temperature. High temperature also favors a larger $NaNbO_3$ crystallite size, the opposite of what is observed for $KNbO_3$, suggesting that the presence of crystalline intermediate phases plays an important role in the nucleation process of the final product. The different crystallization schemes explains the challenge in obtaining stoichiometric $K_{0.5}Na_{0.5}NbO_3$ by hydrothermal synthesis.

Acknowledgements

The study was supported in part by the Danish National Research Foundation (DNRF93). We thank MSc Ola Gjønnes Grendal for his valuable contributions in discussing the results.

References

1. J. Rödel, W. Jo, K. T. P. Seifert, E.-M. Anton and T. Granzow, "Perspective on the Development of Lead-free Piezoceramics", *J. Am. Ceram. Soc.* **92** 1153-77 (2009).
2. Y. Saito, H. Takao, T. Tani, T. Nonoyama, K. Takatori, T. Homma, T. Nagaya and M. Nakamura, "Lead-free Piezoceramics", *Nature* **432** 84-87 (2004).
3. L. Liang, Y. Li, L.-Q. Chen, S. Y. Hu, and G.-H. Lu, "Piezoelectric anisotropy of a KNbO3 single crystal". *J. Appl. Phys.* **108** 094111 (2010).
4. S. K. Mishra, N. Choudhury, S. L. Chaplot, P. S. R. Krishna, and R. Mittal, "Competing antiferroelectric and ferroelectric interactions in $NaNbO_3$: Neutron diffraction and theoretical studies", *Phys. Rev. B* **76** 024110 (2007).
5. K. Byrappa and T. Adschiri, "Hydrothermal technology for nanotechnology", *Prog. Cryst. Growth Charact. Mater.* **53** 117-166 (2007).
6. M.-A. Einarsrud and T. Grande, "1D oxide nanostructures from chemical solutions", *Chem. Soc. Rev.* **43** 2187-99 (2014).
7. A. D. Handoko and G. K. L. Goh, "Hydrothermal synthesis of sodium potassium niobate solid solutions at 200 °C", *Green Chem.* **12** 680-687 (2010).
8. C. Sun, X. Xing, J. Chen, J. Deng, L. Li, R. Yu, L. Qiao, and G. Liu, "Hydrothermal synthesis of single crystalline (K,Na)NbO_3 powders", *Eur. J. Inorg. Chem.* **2007** 1884-88 (2007).
9. G. K. L. Goh, F. F. Lange, S. M. Haile, C. G. Levi, "Hydrothermal synthesis of $KNbO_3$ and $NaNbO_3$ powders". *J. Mater. Res.* **18**, 338-345 (2003).
10. X. Kong, D. Hu, P. Wen, T. Ishii, Y. Tanaka and Q. Feng, "Transformation of potassium Lindquist hexaniobate to various potassium niobates: solvothermal synthesis and structural evolution mechanism", *Dalton Trans*. **42** 7699-7709 (2013).

11. J.-F. Liu, X.-L. Li and Y.-D. Li, “Synthesis and characterization of nanocrystalline niobates“, *J. Cryst. Growth* **247** 419-424 (2003).
12. A. Magrez, E. Vasco, J. W. Seo, C. Dieker, N. Setter and L. Forró, “Growth of Single-Crystalline $KNbO_3$ Nanostructures”, *J. Phys. Chem. B* **110** 58-61(2006).
13. I.C.M.S. Santos, L.H. Loureiro, M.F.P. Silva and Ana M.V. Cavaleiro, “Studies on the hydrothermal synthesis of niobium oxides, *Polyhedron*“, **21** 2009-2015 (2002).
14. S. Y. Wu, W. Zhang and X. M. Chen, “Formation mechanism of $NaNbO_3$ powders during hydrothermal synthesis“, *J. Mater. Sci.: Mater. Electron* **21** 450-455 (2010).
15. H. Zhu, Z. Zheng, X. Gao, Y. Huang, Z. Yan, J. Zou, H. Yin, Q. Zou, S. H. Kable, J. Zhao, Y. Xi, W. N. Martens and R. L. Frost, “Structural Evolution in a Hydrothermal Reaction between Nb_2O_5 and NaOH Solution: From Nb_2O_5 Grains to Microporous $Na_2Nb_2O_6 \cdot {}^2/_3H_2O$ Fibers and $NaNbO_3$ Cubes“, *J. Am. Chem. Soc.* **128** 2373-84 (2006).
16. D. R. Modeshia, R. J. Darton, S. E. Ashbrook, and R. I. Walton, “Control of polymorphism in $NaNbO_3$ by hydrothermal synthesis“, *Chem. Commun.* 68-70 (2009).
17. J.-M. Jehng and I. E. Wachs, “The molecular structures and reactivity of supported niobium oxide catalysts“, *Catal. Today* **8** 37-55 (1990).
18. T. Mokkelbost, Ø. Andersen, R. A. Strøm, K. Wiik, T. Grande, and M.-A. Einarsrud, “High-Temperature Proton-Conducting $LaNbO_4$-Based Materials: Powder Synthesis by Spray Pyrolysis“, *J. Am. Ceram. Soc.* **90** 3395-3400 (2007).
19. Y. Cerenius, K. Ståhl, L. A. Svensson, T. Ursby, A. Oskarsson, J. Albertsson, and A. Liljas, “The crystallography beamline I711 at MAX II“, *J. Synchrotron Rad.* **7** 203-208 (2000).

20. J. Becker, M. Bremholm, C. Tyrsted, B. Pauw, J. Eltzholt, M. Christensen, B. B. Iversen, and K. M. Jensen, “Experimental setup for *in situ* X-ray SAXS/WAXS/PDF studies of the formation and growth of nanoparticles in near- and supercritical fluids“, *J. Appl. Crystallogr.* **43** 729 (2010).
21. K. M. Jensen, M. Christensen, P. Juhas, C. Tyrsted, E. D. Bøjesen, N. Lock, S. J. Billinge, and B. B. Iversen, “Revealing the Mechanisms behind SnO_2 Nanoparticle Formation and Growth during Hydrothermal Synthesis: An in Situ Total Scattering Study”, *J. Am. Chem. Soc.* **134** 6785-92 (2012).
22. A. P. Hammersley, S. O. Svensson, M. Hanfland, A. N. Fitch, and D. Hausermann, “Two-dimensional detector software: From real detector to idealised image or two-theta scan”, *High Pressure Res.* **14** 235248 (1996).
23. P. Thompson, D. E. Cox, and J. B. Hastings, “Rietveld refinement of Debye–Scherrer synchrotron X-ray data from Al_2O_3“, *J. Appl. Cryst.* **20** 79-83 (1987).
24. R. A. Young and P. Desai, “Crystallite size and microstrain indicators in Rietveld refinement”, *Archiwum Nauki o Materialac*h **10** 71 (1989).
25. J. Rodriguez-Carvajal, “Recent advances in magnetic structure determination by neutron powder diffraction“, *Physica B* **192** 55-69 (1993).
26. K. Kato and S. Tamara, "Die Kristallstruktur von T-Nb_2O_5“, *Acta Cryst.* **B31** 673 (1975).
27. A. W. Hewat, “Cubic-tetragonal-orthorhombic-rhombohedral ferroelectric transitions in perovskite potassium niobate: neutron powder profile refinement of the structures“, *J. Phys. C: Solid State Phys.* **6** 2259-72 (1973).
28. G. Philippot, E. D. Bøjesen, C. Elissalde, M. Maglione, C. Aymonier and B. B. Iversen, “Insights into $BaTi_{1-y}Zr_yO_3$ ($0 \leq y \leq 1$) Synthesis under Supercritical Fluid Conditions“, *Chem. Mater.* **28** 3391-3400 (2016).

29. G. Shirane, H. Danner, A. Pavlovic, and R. Pepinsky, “Phase Transitions in Ferroelectric $KNbO_3$“, *Phys. Rev.* **93** 672-673 (1954).

30. G. Wang, S. M. Selbach, Y. Yu, X. Zhang, T. Grande, and M.-A. Einarsrud, “Hydrothermal synthesis and characterization of $KNbO_3$ nanorods”, *CrystEngComm* **11** 195863 (2009).

31. T. M. Anderson, M. A. Rodriguez, F. Bonhomme, J. N. Bixler, T. M. Alam and M. Nyman, “An aqueous route to $[Ta_6O_{19}]^{8-}$ and solid-state studies of isostructural niobium and tantalum oxide complexes“, *Dalton Trans.* **2007** 4517-22 (2007).

32. H. Xu, M. Nyman, T. M. Nenoff and A. Navrotsky, “Prototype Sandia Octahedral Molecular Sieve (SOMS) $Na_2Nb_2O_6 \cdot H_2O$: Synthesis, Structure and Thermodynamic Stability”, *Chem. Mater.* **16** 2034-40 (2004).

33. M. D. Peel, S. P. Thompson, A. Daoud-Aladine, S. E. Ashbrook, and P. Lightfoot, “New Twists on the Perovskite Theme: Crystal Structures of the Elusive Phases R and S of $NaNbO_3$“, *Inorg. Chem.* **51** 6876-89 (2012).

Figure captions

Figure 1 a) 2D contour plot (Colors red-yellow-blue in Figure 1a show intensity from high to low. Black tics=T-Nb_2O_5 and red tics=$KNbO_3$), b) single diffraction patterns at different heating times showing the development of phases during hydrothermal synthesis of $KNbO_3$ at 275 °C and 250 bar, c) Rietveld refinement of the final $KNbO_3$ product phase (space group Pmmn) and d) the extracted scale factor for $KNbO_3$ from sequential Rietveld refinements for the experiments at 250, 275 and 300 ˚C.

Figure 2 a) Crystallite size and b) evolution of tetragonality for the growing $KNbO_3$ particles at various synthesis temperatures. The two contributions were refined independently of one another.

Figure 3 Integrated area of the broad background features as a function of heating time for various temperatures in the 2θ-range a) 5-13° and b) 13-37°.

Figure 4 a) 2D contour plot with guidelines showing the development stages 1-5 during hydrothermal synthesis of $NaNbO_3$ at 225 °C and 250 bar (colors red-yellow-blue show intensity from high to low; Black tics=T-Nb_2O_5, blue tics= $Na_7HNb_6O_{19}\cdot 15H_2O$ and red tics=$NaNbO_3$) and b) crystallite size over time for $Na_2Nb_2O_6\cdot H_2O$ at 225 °C and 250 bar and c) Rietveld refinement (space group Pmmn) of final reaction product $NaNbO_3$.

Figure 5 a) The time to complete conversion to $NaNbO_3$ at different reaction temperatures and b) crystallite size of $NaNbO_3$ at various temperatures and 250 bar.

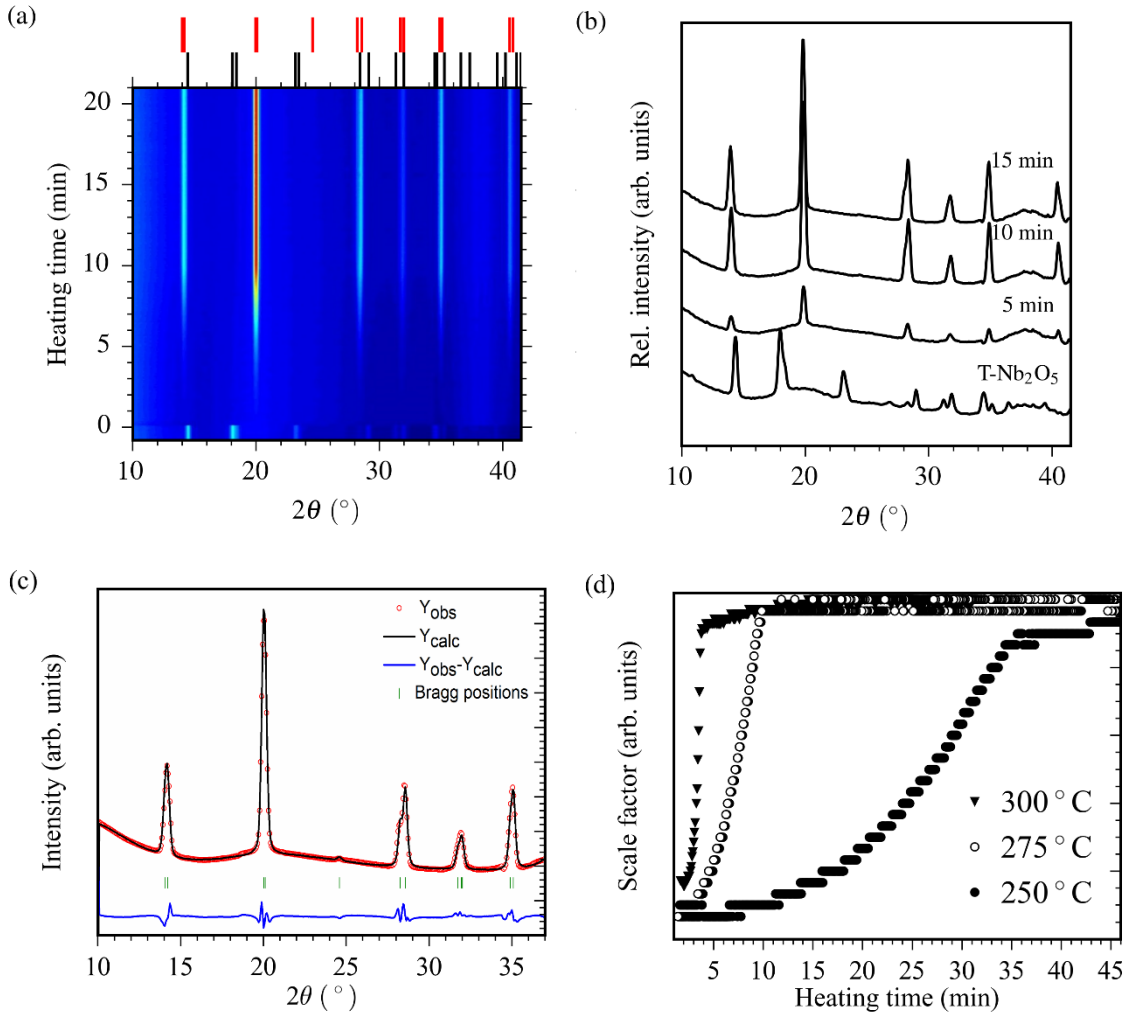
(a)
Heating time (min)
2θ (°)
(b)
Rel. intensity (arb. units)
15 min
10 min
5 min
T-Nb2O5
2θ (°)
(c)
Intensity (arb. units)
Yobs
Ycalc
Yobs-Ycalc
Bragg positions
2θ (°)
(d)
Scale factor (arb. units)
300 °C
275 °C
250 °C
Heating time (min)

(a)

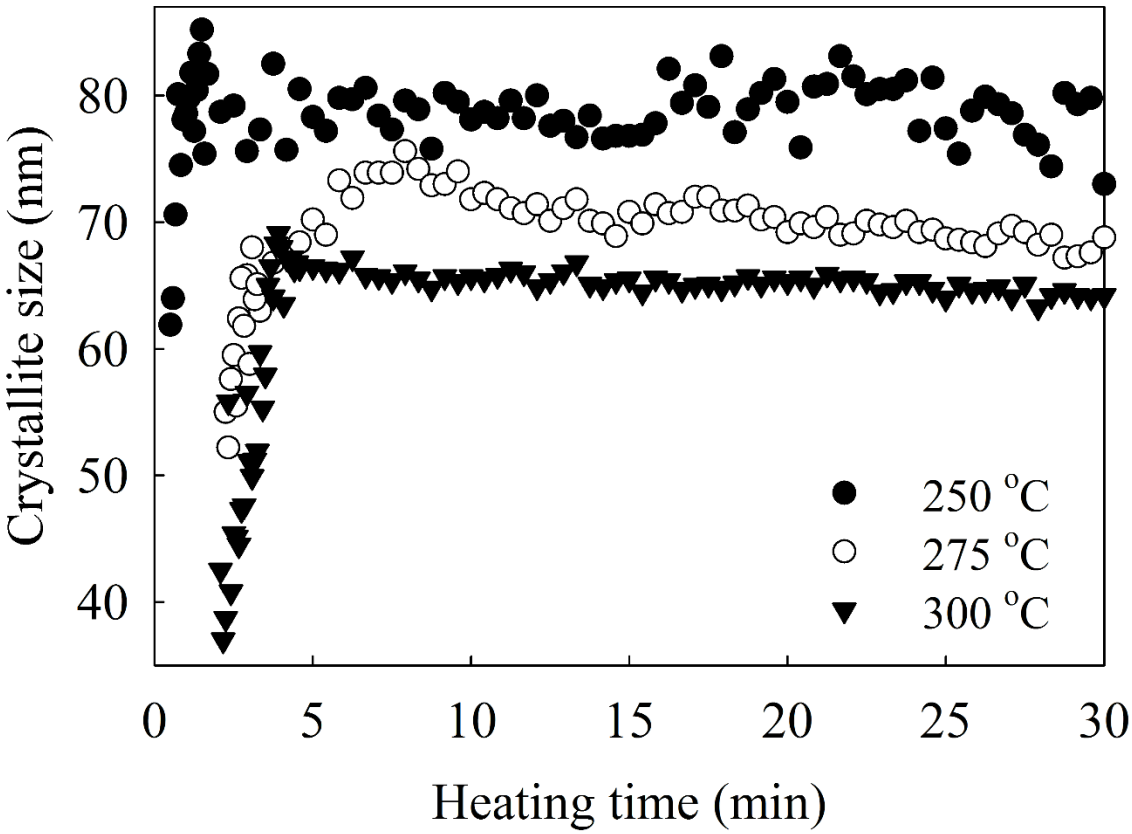
Crystallite size (nm)
80
70
60
50
40
0
5
10
15
20
25
30
Heating time (min)
250 °C
275 °C
300 °C

(b)

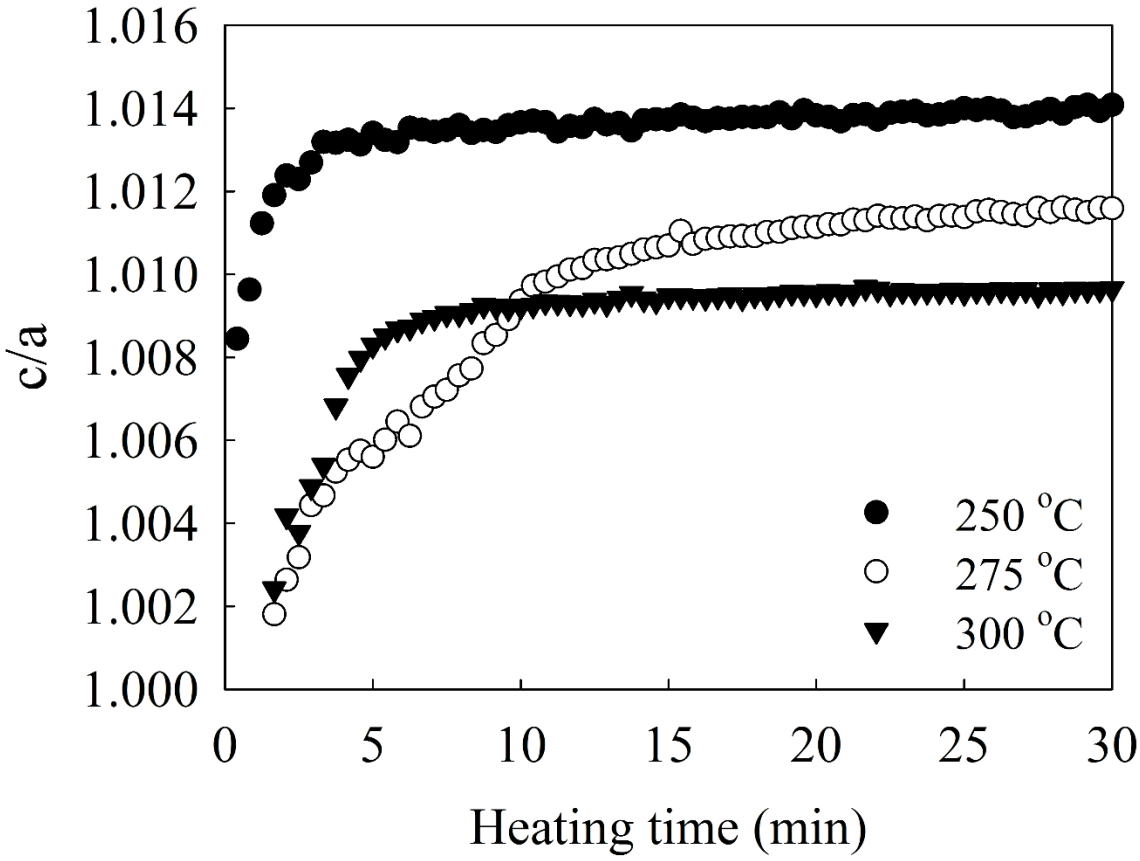
1.016
1.014
1.012
1.010
1.008
1.006
1.004
1.002
1.000
c/a
0
5
10
15
20
25
30
Heating time (min)
250 °C
275 °C
300 °C

(a)

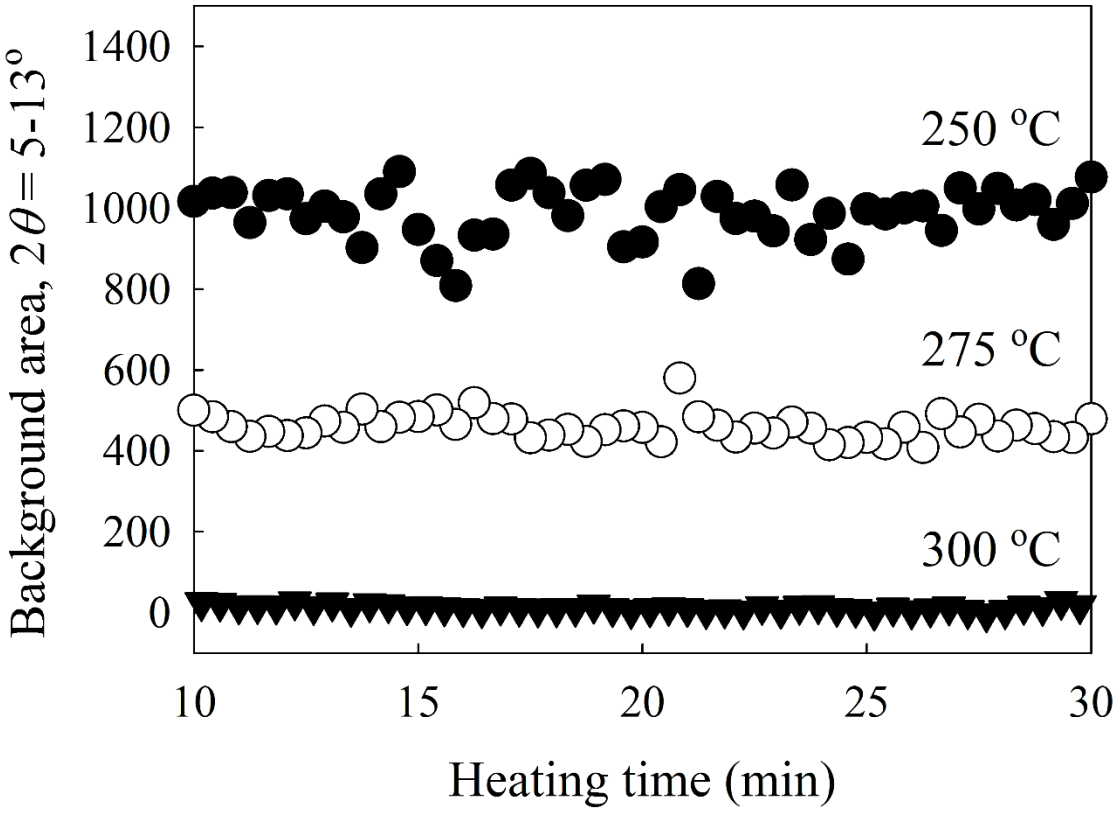
1400
1200
1000
800
600
400
200
0
Background area, 2θ= 5-13°
10
15
20
25
30
Heating time (min)
250 °C
275 °C
300 °C

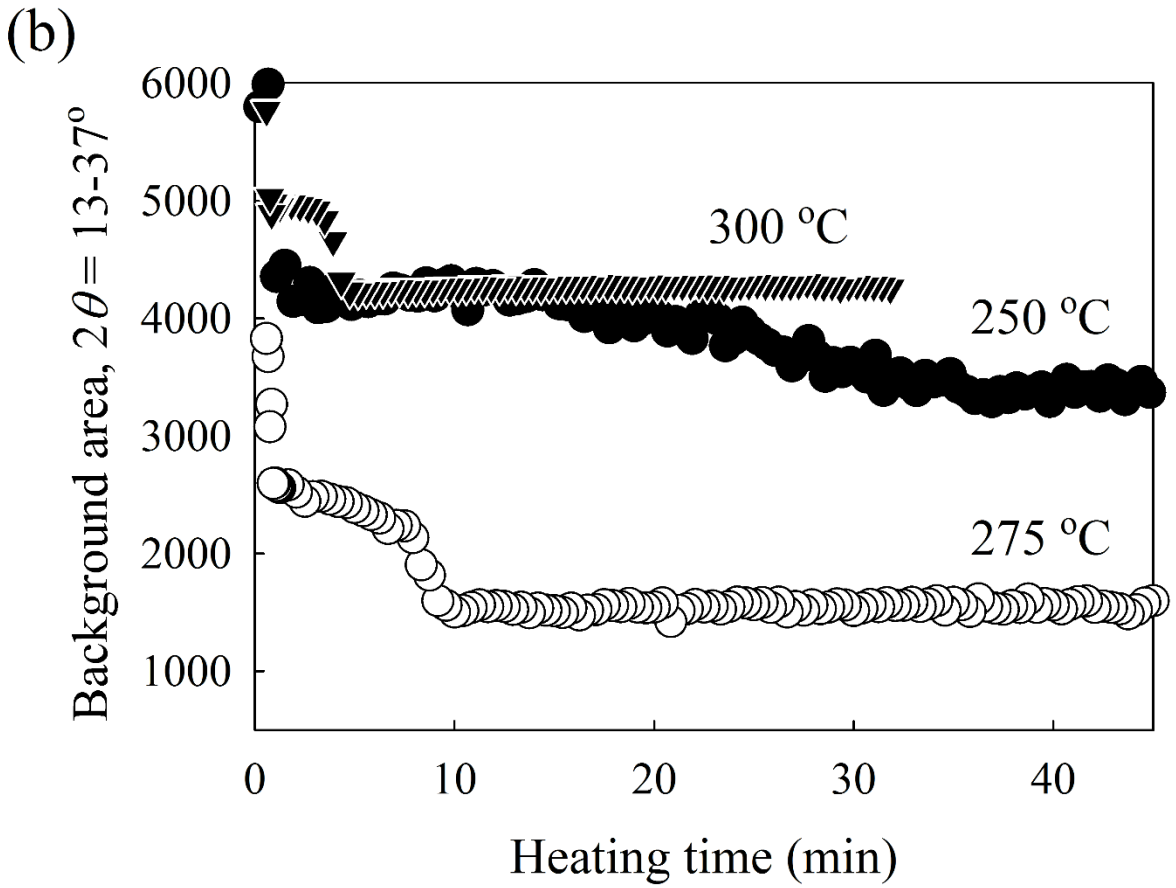
(b)
Background area, 2θ = 13-37°
6000
5000
4000
3000
2000
1000
300 °C
250 °C
275 °C
0
10
20
30
40
Heating time (min)

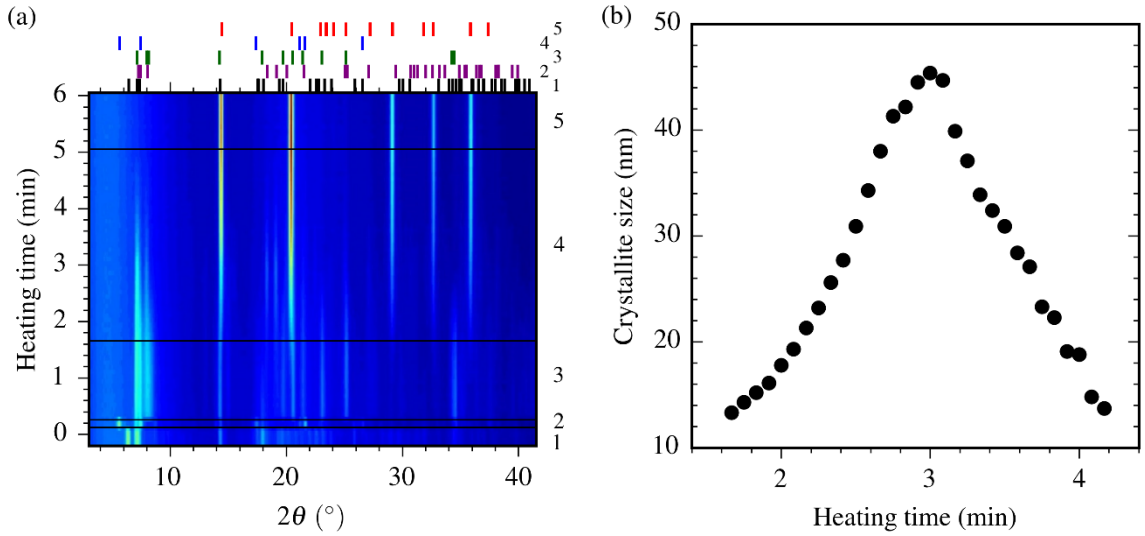
(a)
Heating time (min)
2θ (°)
(b)
Crystallite size (nm)
Heating time (min)

(c)

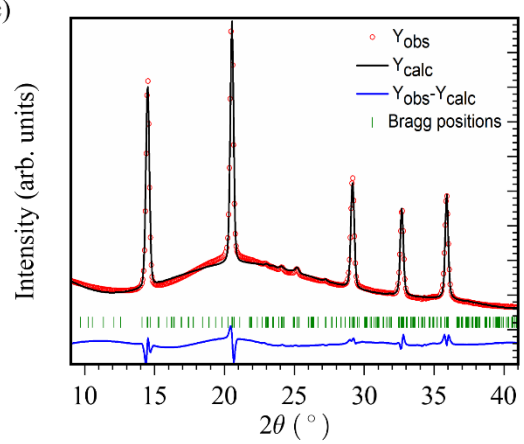
Yobs
Ycalc
Yobs-Ycalc
Bragg positions
Intensity (arb. units)
10
15
20
25
30
35
40
2θ (°)

(a)

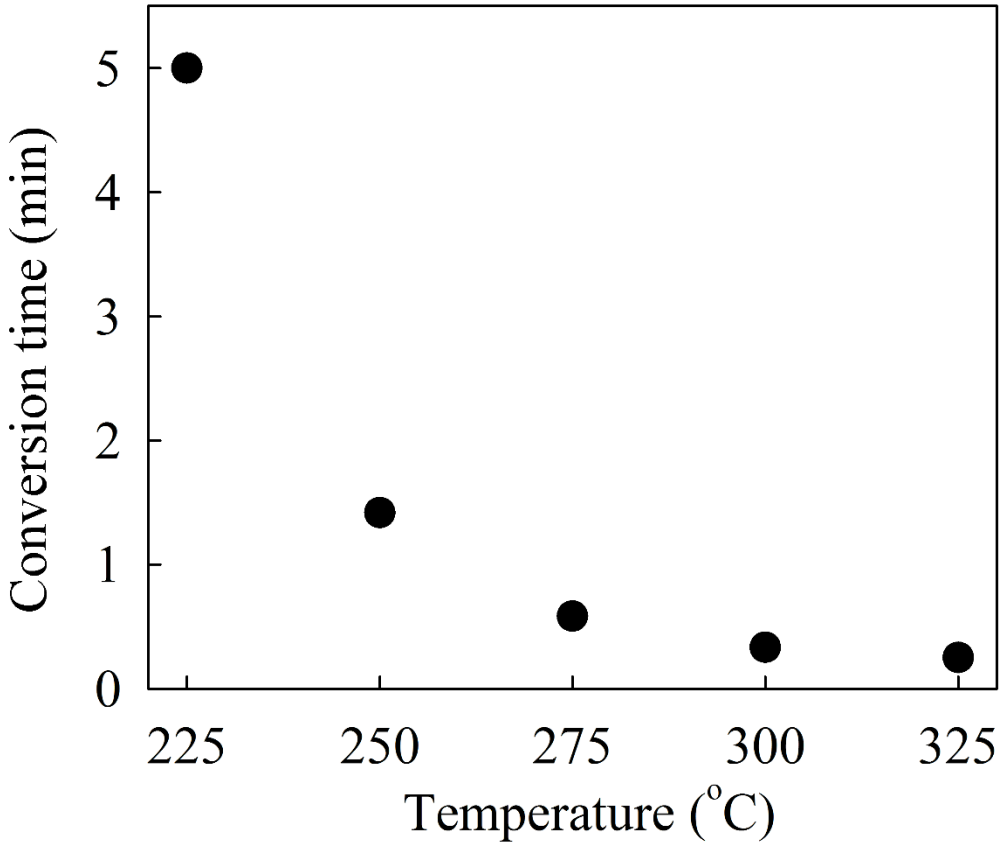
Conversion time (min)
0
1
2
3
4
5
225
250
275
300
325
Temperature (°C)

(b)

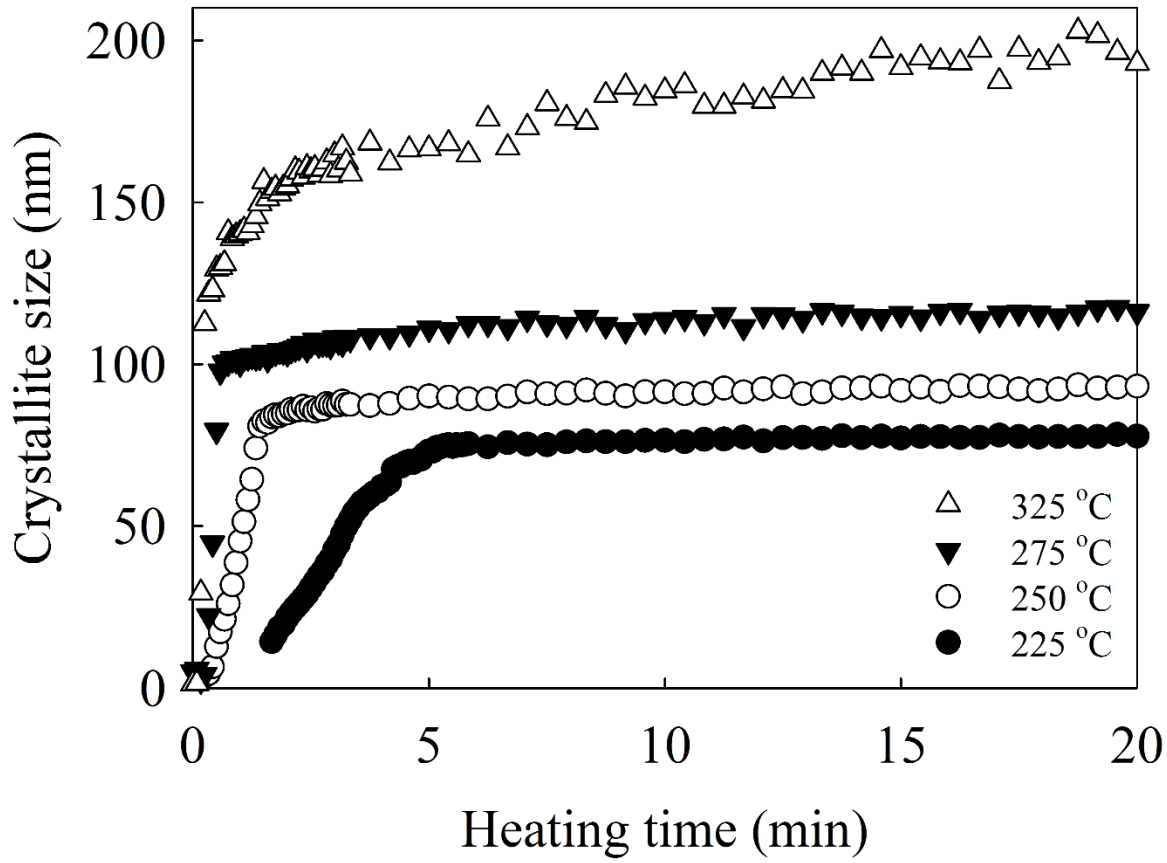
Crystallite size (nm)
200
150
100
50
0
0
5
10
15
20
Heating time (min)
325 °C
275 °C
250 °C
225 °C